catalysts

MDPI

Article

Synthesis of Au–Cu Alloy Nanoparticles as Peroxidase Mimetics for H_2O_2 and Glucose Colorimetric Detection

Cun Liu [1], Sang Hyuk Im [2,*] and Taekyung Yu [1,*]

[1] Department of Chemical Engineering, Kyung Hee University, Yongin 17104, Korea; cunliu@khu.ac.kr
[2] Department of Chemical and Biological Engineering, Korea University, Seoul 02841, Korea
* Correspondence: imromy@korea.ac.kr (S.H.I.); tkyu@khu.ac.kr (T.Y.)

Abstract: The detection of hydrogen peroxide (H_2O_2) is essential in many research fields, including medical diagnosis, food safety, and environmental monitoring. In this context, Au-based bimetallic alloy nanomaterials have attracted increasing attention as an alternative to enzymes due to their superior catalytic activity. In this study, we report a coreduction synthesis of gold–copper (Au–Cu) alloy nanoparticles in aqueous phase. By controlling the amount of Au and Cu precursors, the Au/Cu molar ratio of the nanoparticles can be tuned from 1/0.1 to 1/2. The synthesized Au–Cu alloy nanoparticles show good peroxidase-like catalytic activity and high selectivity for the H_2O_2-mediated oxidation of 3,3′,5,5′-tetramethylbenzidine (TMB, colorless) to TMB oxide (blue). The Au–Cu nanoparticles with an Au/Cu molar ratio of 1/2 exhibit high catalytic activity in the H_2O_2 colorimetric detection, with a limit of detection of 0.141 μM in the linear range of 1–10 μM and a correlation coefficient R^2 = 0.991. Furthermore, the Au–Cu alloy nanoparticles can also efficiently detect glucose in the presence of glucose oxidase (GOx), and the detection limit is as low as 0.26 μM.

Keywords: Au–Cu alloy nanoparticles; peroxidase mimetic; H_2O_2 colorimetric detection

check for updates

Citation: Liu, C.; Im, S.H.; Yu, T. Synthesis of Au–Cu Alloy Nanoparticles as Peroxidase Mimetics for H_2O_2 and Glucose Colorimetric Detection. *Catalysts* **2021**, *11*, 343. https://doi.org/10.3390/catal11030343

Academic Editors: Leonarda Francesca Liotta and Sónia Carabineiro

Received: 29 January 2021
Accepted: 5 March 2021
Published: 7 March 2021

1. Introduction

Hydrogen peroxide (H_2O_2), an essential representative of reactive oxygen species, plays a critical role in various biological processes, including cell proliferation, differentiation, and migration [1–3]. Moreover, H_2O_2 is a vital component in modern industries applications such as chemical synthesis, water treatment, and textile bleaching, in which H_2O_2 is used as a versatile and environmentally benign oxidant [4,5]. Meanwhile, H_2O_2 is also a byproduct of many enzymatic reactions in living beings. The generation and accumulation of H_2O_2 may cause several diseases, e.g., cancer, Alzheimer's disease, and Parkinson's disease, endangering the health and life of human beings [6]. Therefore, the detection of H_2O_2 is essential in various areas including medical diagnosis, food safety, and environmental monitoring [7–9].

In terms of H_2O_2 detection, numerous analytical strategies have been developed, such as optical sensing, electrochemical analysis, and colorimetric methods [10–13]. Among these, colorimetric methods show great potential in practical applications due to advantages including simplicity, low cost, and unsophisticated instrumentation [14–17]. In colorimetric assays, a natural enzyme is typically needed to develop an optical signal. However, practical applications of natural enzymes are restricted by their high cost and low stability against denaturation and protease [18,19]. Consequently, many studies have been devoted to the development of alternative approaches based on nanozymes, whose intrinsic properties such as large specific surface area, high stability, good durability, low cost, and tunable catalytic activity render them suitable for various practical applications [20–22]. Since the first Fe_3O_4-based nanozyme was reported [23], several kinds of nanomaterials have been developed, e.g., metallic oxide nanoparticles [24–27], carbon-based nanomaterials [28,29], and noble metal nanoparticles (Au, Ag, and Pt) [30–33].

Among these nanomaterials, Au nanoparticles are often used in fundamental research due to their good enzyme-like activities as both oxidase and peroxidase mimics [34]. However, naked Au nanoparticles generally show high chemical inertness in many catalytic reactions of enzyme mimics [35]. Moreover, aggregation of Au nanoparticles often occurs, reducing their catalytic efficiency and hampering their practical application. To circumvent these problems, Au-based bimetallic alloy nanomaterials have attracted significant attention because of their superior catalytic activity to that of their single-phase counterparts [36,37]. For example, Zhang et al. prepared Au–Ag alloy nanoboxes, which can be employed to detect H_2O_2 with a linear readout in a range of concentration from 5×10^{-2} M down to 5×10^{-7} M [38]. Li et al. developed Au–Pd bimetallic nanoparticles using a facile thermal coreduction method that exhibited linear responses of H_2O_2 in concentration ranges of 0.8 μM to 10 mM, with a limit of detection (LOD) of 0.16 μM [39]. Sui et al. synthesized an Au–Hg amalgam by introducing Hg^{2+} into Au nanoparticles, which showed an enhanced peroxidase-mimicking activity toward H_2O_2 and Hg^{2+} in a sensitive and selective method for colorimetric detection. The LOD was as low as 0.35 μM for H_2O_2 [40]. As can be extracted from these reports, Au-based bimetallic alloy nanomaterials with good dispersion degree and excellent enzyme-like performance are relevant for H_2O_2 detection in various research fields.

In this paper, we report a coreduction method for the synthesis of well-mixed Au–Cu alloy nanoparticles in aqueous phase, in which the Au/Cu ratio can be tuned from 1/0.1 to 1/2 by controlling the amount of Au and Cu precursors. In a typical colorimetric reaction, that is, the H_2O_2-mediated oxidation of the peroxidase substrate 3,3′,5,5′-tetramethylbenzidine (TMB, colorless) to produce TMB oxide (TMBox, blue), the prepared Au–Cu alloy nanoparticles showed good peroxidase-mimicking catalytic activity. Meanwhile, using various common ions and substances as controls, the high selectivity in H_2O_2 detection of the synthesized Au–Cu alloy nanoparticles was demonstrated.

2. Results and Discussion

2.1. Characterization of Au–Cu Alloy Nanoparticles

The Au–Cu alloy nanoparticles were synthesized by coreducing Au and Cu precursors using L-ascorbic acid (AA) in the presence of poly(ethyleneimine) (PEI) solution in an aqueous phase system. The solution color changed from chartreuse to maroon after adding AA, which indicated the formation of nanoparticles. In this synthesis process, PEI served as a surfactant for the formation of nanosized particles and as a stabilizing agent to prevent the oxidation of Cu species in the nanoparticles [41,42]. By varying the amount of Au and Cu precursors, the molar ratio between Au and Cu in the nanoparticles was controlled from 1/0.1 ($Au_1Cu_{0.1}$) to 1/2 (Au_1Cu_2), as determined by inductively coupled plasma (ICP) (Table S1). The transmission electron microscopy (TEM) images of the nanoparticles depicted in Figure 1a–e revealed that the synthesized nanoparticles had a quasispherical morphology and an average size of around 62.4 nm for $Au_1Cu_{0.1}$, 63.2 nm for $Au_1Cu_{0.2}$, 64.8 nm for $Au_1Cu_{0.5}$, 79.5 nm for Au_1Cu_1, and 101.3 nm for Au_1Cu_2 (Figure S1). The elemental distribution of the nanoparticles was also analyzed by energy-dispersive X-ray spectrometry (EDS) mapping, which indicated that Au and Cu were well dispersed in the Au–Cu alloy nanoparticles (Figure S2). Figure 1f shows the powder X-ray diffraction (XRD) patterns of the nanoparticles with different Au/Cu molar rations, which indicate that all the nanoparticles had an alloy structure based on Au (Joint Committee on Powder Diffraction Standards (JCPDS) file card no. 04-0784) rather than Cu (JCPDS file card no. 04-0836). In the XRD patterns, all XRD peaks exhibited most likely were due to the insertion of small Cu atoms in the Au crystal lattice, and no XRD peaks of Cu or CuO were observed. [43] In addition, the UV-VIS absorption spectrum exhibited the characteristic absorption of Au–Cu alloy nanoparticles with different Au/Cu molar ratio in the UV region (Figure S3) These observations demonstrated that the Au–Cu nanoparticles formed an alloy structure and were well stabilized in the aqueous solution, and that no aggregation occurred.

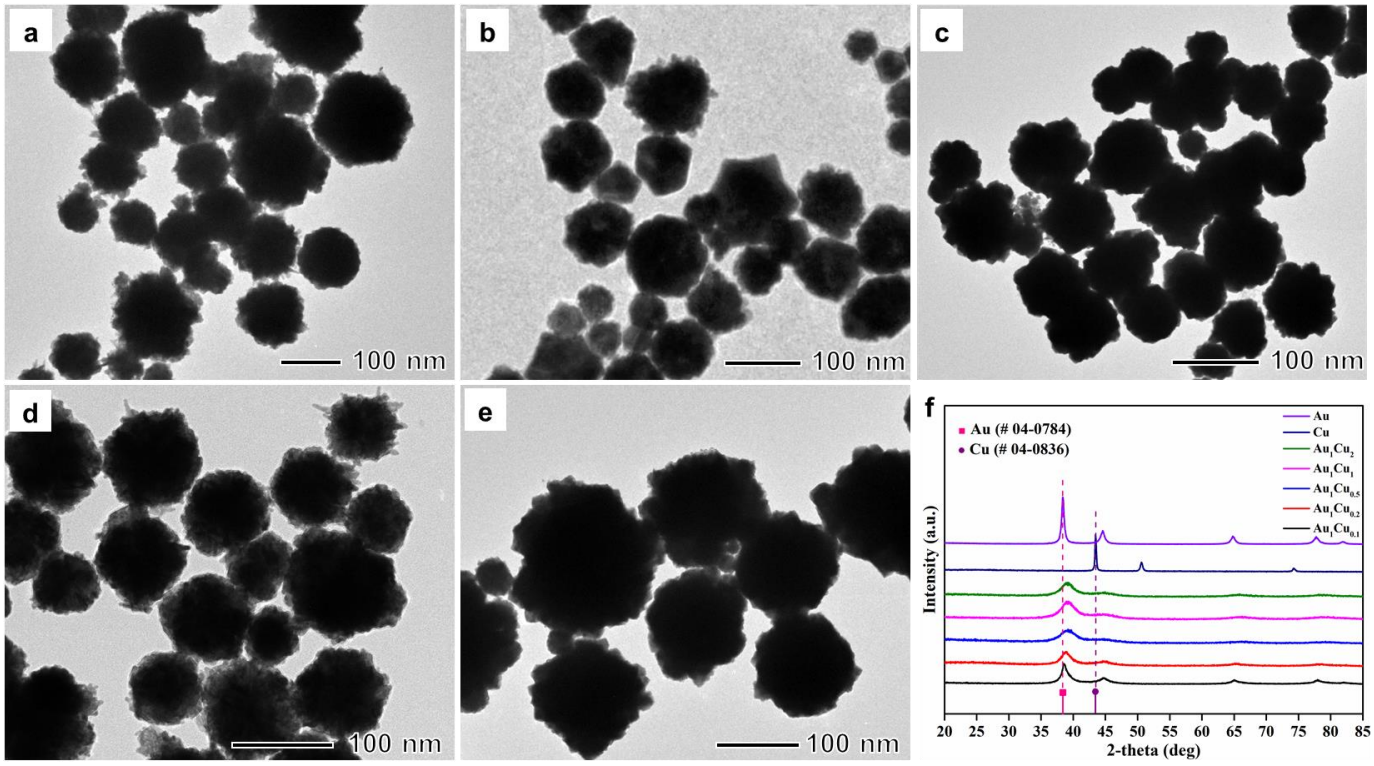

Figure 1. Transmission electron microscopy images of (**a**) $Au_1Cu_{0.1}$, (**b**) $Au_1Cu_{0.2}$, (**c**) $Au_1Cu_{0.5}$, (**d**) Au_1Cu_1, and (**e**) Au_1Cu_2 alloy nanoparticles. (**f**) X-ray diffraction patterns of the Au–Cu alloy nanoparticles.

2.2. H_2O_2 Detection

In previous reports, the peroxidase-like catalytic properties of Au-based alloy nanoparticles have been explored by different detection strategies. In the present work, we performed the catalytic activity analysis of the prepared Au–Cu alloy nanoparticles by colorimetric method using TMB as a chromogenic substrate [44]. As previous reported, the catalytic activity of enzyme-mimicking nanoparticles is dependent on pH and temperature. Thus, the catalytic activity of the Au–Cu nanoparticles was investigated under different pH and temperature conditions. The reaction solution pH- and temperature-dependent curves are shown in Figures 2 and 3. The results show that the highest absorbance intensities were at pH = 4 and room temperature, respectively. Accordingly, under these conditions, we confirmed that there was no reaction in the absence of the Au–Cu alloy nanoparticles (Figure 4). When the reaction was conducted in the presence of the Au–Cu alloy nanoparticles, the intensity of the absorbance peak at around 652 nm increased, which is characteristic of TMBox, and indicated that the synthesized Au–Cu alloy nanoparticles possessed catalytic activity in TMB oxidation by generating OH radicals from H_2O_2, thereby causing the color change.

Monitoring of the UV-VIS absorption-peak evolution of the TMB reaction solutions containing $Au_1Cu_{0.1}$, $Au_1Cu_{0.2}$, $Au_1Cu_{0.5}$, Au_1Cu_1, and Au_1Cu_2 showed that the UV-VIS absorbance intensity increased with the H_2O_2 concentrations (Figure 5a–e and Figure S4). Wide detection ranges from 1 μM to 10 mM was observed for all Au–Cu alloy nanoparticles. According to the equation LOD = 3δ/k [45], where δ is the standard deviation of 10 replicate measurements of absorbance of the blank signal (absorbance of TMB solution without H_2O_2), and k is the slope of the calibration curve, the LODs for H_2O_2 were calculated to be 0.609 μM for $Au_1Cu_{0.1}$, 0.508 μM for $Au_1Cu_{0.2}$, 0.274 μM for $Au_1Cu_{0.5}$, 0.178 μM for Au_1Cu_1, and 0.141 μM for Au_1Cu_2. The lowest LOD of Au_1Cu_2 may be related to the increase in Cu content, since many reports have demonstrated that not only Au, but also Cu^+ nanomaterials possess peroxidase activity [46]. In addition, a comparison with other

nanomaterials exhibiting activity for H_2O_2 detection demonstrated that the present Au–Cu alloy nanoparticles had low LOD and a wide detection range (Table 1).

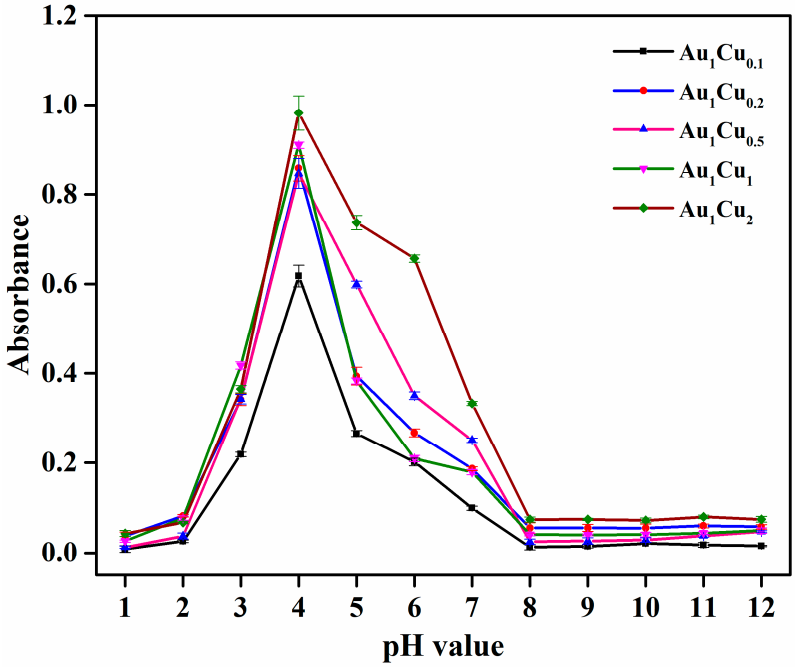

Figure 2. The pH-dependent response curve for H_2O_2 detection using the as-prepared Au–Cu alloy nanoparticles incubated at room temperature. The error bars represent the standard deviation of three measurements.

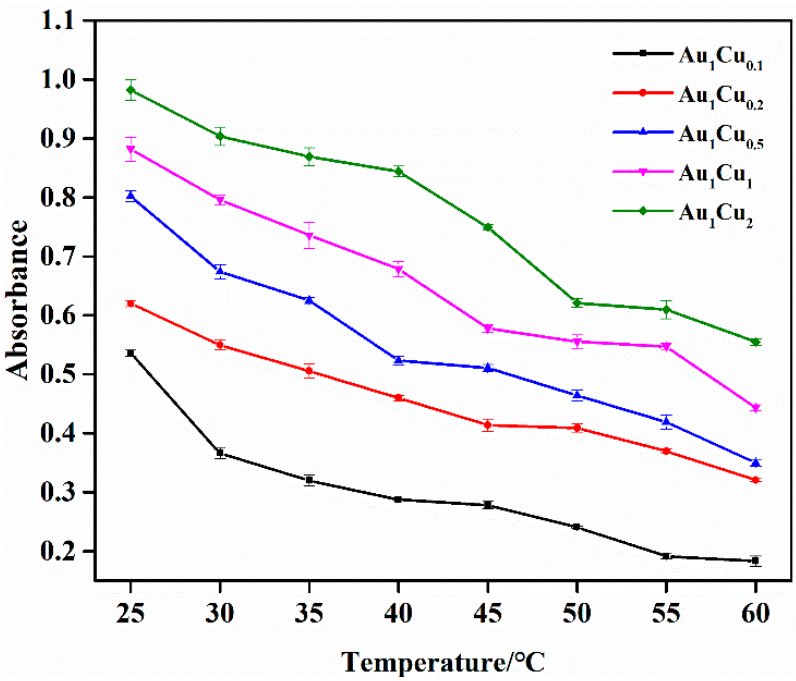

Figure 3. Temperature-dependent response curve for H_2O_2 detection using the as-prepared Au–Cu alloy nanoparticles at pH = 4. The error bars represent the standard deviation of three measurements.

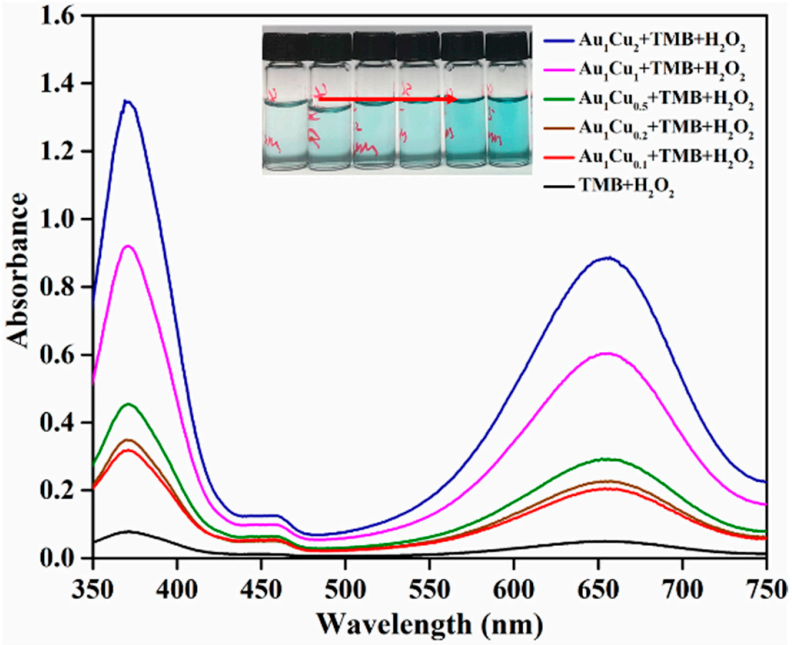

Figure 4. Ultraviolet-visible absorption spectra of 3,3′,5,5′-tetramethylbenzidine (TMB) in different reaction systems.

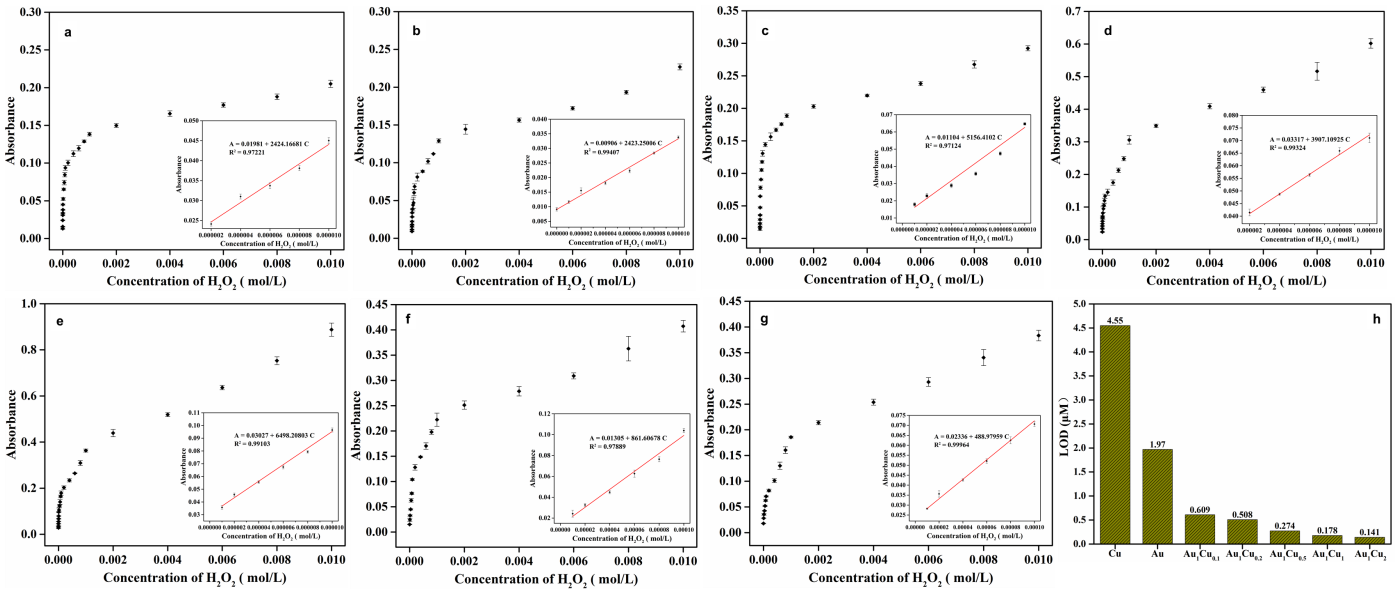

Figure 5. (**a**–**g**) Dose-response curves for H_2O_2 detection using (**a**) $Au_1Cu_{0.1}$, (**b**) $Au_1Cu_{0.2}$, (**c**) $Au_1Cu_{0.5}$, (**d**) Au_1Cu_1, (**e**) Au_1Cu_2, (**f**) Cu, and (**g**) Au as peroxidase mimetics. Inset of (**a**)–(**e**): Linear range of absorbance intensity versus H_2O_2 concentration. (**h**) Limit of detection (LOD) for H_2O_2 of $Au_1Cu_{0.1}$, $Au_1Cu_{0.2}$, $Au_1Cu_{0.5}$, Au_1Cu_1, Au_1Cu_2 nanoparticles, Cu nanoparticles, and Au nanoparticles.

To gain more insight into the catalytic properties of the Au–Cu alloy nanoparticles, we also prepared single Au nanoparticles and Cu nanoparticles by coreduction (Figure S5) and detected their catalytic activity under the same conditions, as shown in Figure 5f,g and Figure S6. The LOD of the Au nanoparticles and Cu nanoparticles were 1.97 μM and 4.55 μM, respectively, in the linear range of 10–100 μM. Therefore, it can be concluded that the Au–Cu alloy nanoparticles had a wider detection range and a lower LOD than the single derivatives (Figure 5h), indicating that the formation of the Au–Cu alloy is beneficial for peroxidase-like activity.

Table 1. Analytical parameters of H_2O_2 detection in recent papers.

Material	Detection Range (μM)	LOD (μM)	References
Por–CeO_2	10–100	1.8	[16]
Au–Hg	5–100	0.35	[40]
Au@TiO_2	5–400	4.0	[47]
Au/Co_3O_4–CeO_x	10–1000	5.29	[48]
FePt–Au	20–700	12.33	[49]
AuNPs@AuNCs	50–2500	30	[50]
FeS_2	80–200	0.91	[51]
Au@Ag	0–100	3.2	[52]
Au–Cu	1–1000	0.141	This work

2.3. Selectivity Analysis

The catalytic performance of enzymes is determined by their selectivity and sensitivity for the detection of target substrates; therefore, the selectivity of enzyme mimetics is worth investigating. In this study, to determine the detection selectivity of the Au–Cu alloy nanoparticles for H_2O_2, we performed control experiments using various common ions (Na^+, K^+, Ca^{2+}, Mg^{2+}, PO_4^{3-}, and Cl^-) and other substances (AA, glucose, and urea). These ions and substances can be usually found in human plasma and might influence the catalytic activity of the Au–Cu alloy nanoparticles. As shown in Figure 6, these controls generated negligible UV-VIS absorbance compared with H_2O_2 in the colorimetric reaction, which is indicative of the high selectivity of the Au–Cu alloy nanoparticles for H_2O_2 detection. In contrast, the tested ions, ascorbic acid, glucose, and urea, cannot directly generate $^{\bullet}OH$ radicals from H_2O_2 for TMB oxidation. As for glucose, the Au–Cu alloy nanoparticles may also exhibit peroxidase-mimicking activity in the presence of glucose oxidase (GO_x), because the GOx can decompose glucose to generate H_2O_2, thereby causing the colorimetric reaction in the presence of Au–Cu alloy nanoparticles. Therefore, we performed the comparison of absorbance intensity between TMB solution in the absence and in the presence of GO_x by the colorimetric method, as shown in Figure 7. The results showed enhanced absorbance intensity in the presence of GO_x, indicating that glucose detection can be performed in the presence of GO_x.

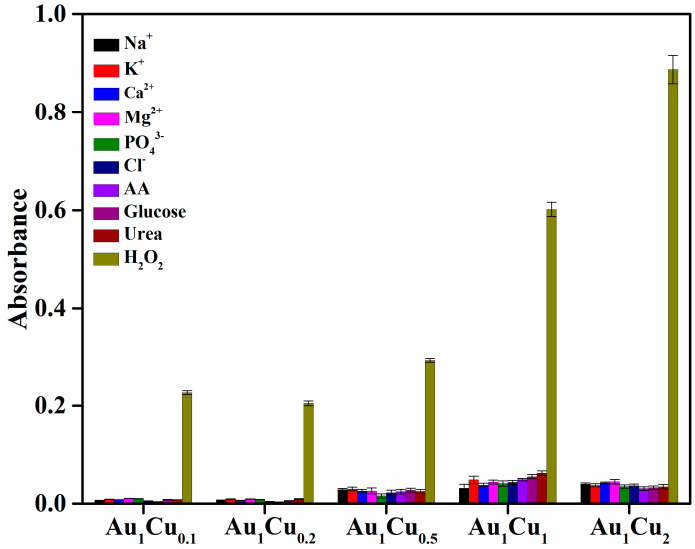

Figure 6. Selectivity analysis of H_2O_2 detection using Au–Cu alloy nanoparticles as peroxidase mimetics. The concentration of H_2O_2 and other substances was 10 mM.

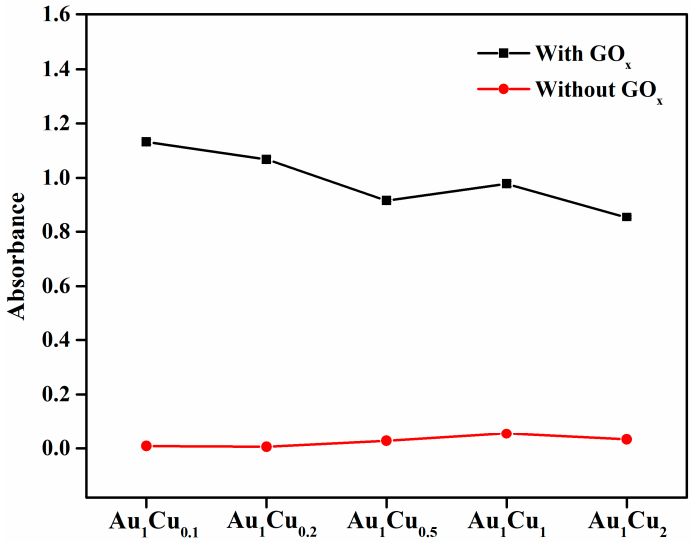

Figure 7. Ultraviolet-visible absorption intensity of 3,3′,5,5′-tetramethylbenzidine (TMB) in the presence of glucose with and without glucose oxidase (GO_X). The concentration of glucose was 10 mM.

2.4. Glucose Detection and Selectivity Analysis

Glucose oxidase (GOx) can promote the catalytic oxidation of glucose to produce H_2O_2. Therefore, the Au–Cu-based colorimetric method can be used for glucose detection in the presence of GOx. The typical UV-VIS absorption spectra of the TMB reaction solutions and glucose-concentration response curve for Au–Cu are shown in Figure 8 and Figure S7. The prepared Au–Cu alloy nanoparticles showed the lowest detection limit of 2.6×10^{-7} mol/L in the linear range of 2 to 10 μM for glucose detection, which was superior to that of several previously reported artificial enzymes (Table 2). Furthermore, the selectivity of glucose detection was investigated via control experiments. Several typical common glucose homologues (sucrose, lactose, maltose, and mannitol) and glucose were comparatively analyzed, and the results are presented in Figure 9. The absorption intensity was clearly higher in the presence of glucose than those of the control samples, indicating that the proposed Au–Cu based system exhibited high selectivity for glucose detection.

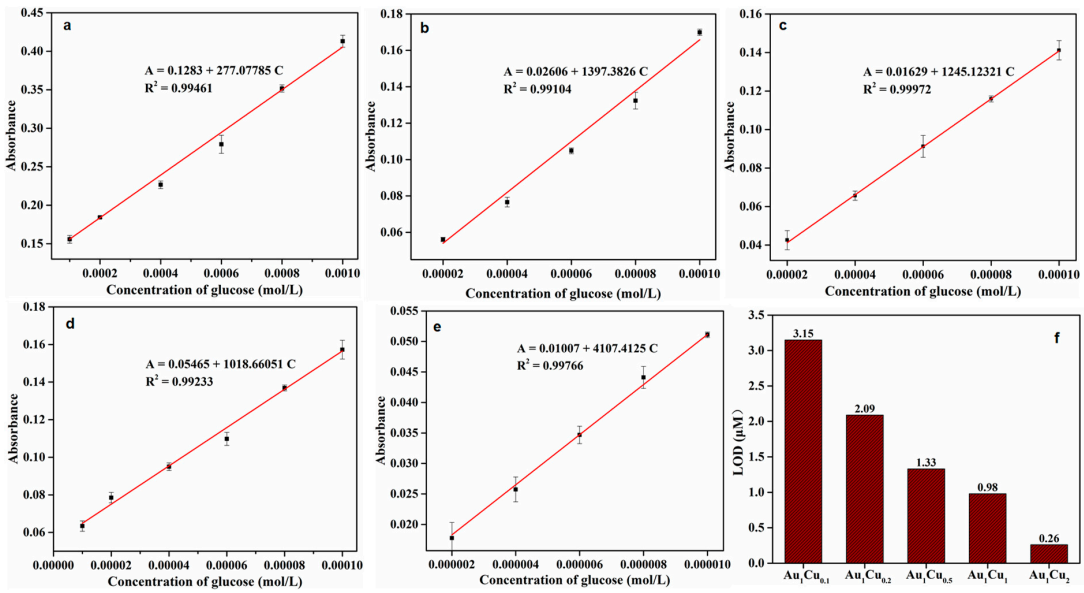

Figure 8. (**a**–**e**) Dose-response curves for glucose detection using (**a**) $Au_1Cu_{0.1}$, (**b**) $Au_1Cu_{0.2}$, (**c**) $Au_1Cu_{0.5}$, (**d**) Au_1Cu_1, and (**e**) Au_1Cu_2 as peroxidase mimetics. Inset of **a**–**e**: Linear range of absorbance intensity versus H_2O_2 concentration. (**f**) Limit of detection (LOD) for glucose of $Au_1Cu_{0.1}$, $Au_1Cu_{0.2}$, $Au_1Cu_{0.5}$, Au_1Cu_1, and Au_1Cu_2 nanoparticles.

Table 2. Analytical parameters of glucose detection in recent papers.

Material	Detection Range (μM)	LOD (μM)	References
R–Co_3O_4	0.001–0.02	0.32	[53]
Pd–Cu	1–30	1.9	[54]
Pd–Ni	1–25	1.9	[55]
branched Au–Cu	0.25–10	16.62	[56]
Au–Ni	0.001–30	0.29	[57]
Pt–Au	0.01–10	3	[58]
Au_1Cu_2	0.002–0.01	0.26	This work

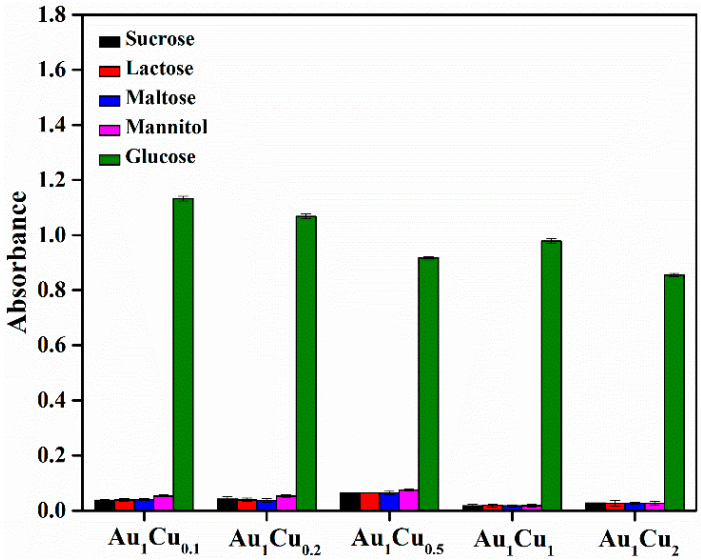

Figure 9. Selectivity analysis of glucose detection using Au–Cu alloy nanoparticles as peroxidase mimetics. The concentration of glucose and other substances was 10 mM.

3. Materials and Methods

3.1. Materials

Copper sulfate ($CuSO_4$), gold (III) chloride trihydrate ($HAuCl_4 \cdot 3H_2O$), AA, and PEI (Mw = 75000) were purchased from Sigma-Aldrich (St. Louis, MO, USA) and used to synthesize the Au–Cu alloy nanoparticles. Sodium acetate (NaAc), acetic acid, TMB, H_2O_2 (30 wt %), HEPES, glucose, and GO_x were also purchased from Sigma-Aldrich and used in the peroxidase activity assay.

3.2. Characterization

A D8 Advance X-ray diffractometer (XRD) was used for the crystal-structure characterization of the Au–Cu alloy nanoparticles. For the morphological characterization, transmission electron microscopy (TEM) was performed using a JEM-2100F, JEOL microscope. The energy-dispersive X-ray spectrometry (EDS) analysis was performed using a JEM-2100F microscope operated at 200 kV for the elemental analysis. The UV-VIS absorption spectra were acquired using a Cary 60 UV-VIS spectrophotometer (Agilent Technologies, Santa Clara, CA, USA). An inductively coupled plasma spectrometer (Direct Reading Echelle ICP, LEEMAN, Hudson, NH, USA) was used to determine the Au/Cu molar ratio in the nanoparticles.

3.3. Preparation of Au–Cu Alloy Nanoparticles

A total of 10 mL of reaction system was prepared. First, an aqueous solution containing 10 mg of PEI was heated to 90 °C with magnetic stirring. Then, aqueous $CuSO_4$ solution (0.1 M) and $HAuCl_4$ solution (0.1 M) with different volumes were added to the PEI solution. After 5 min, 3 mL of AA (0.6 M) was added to the reaction mixture, and the resulting

solution was heated at the same temperature for 5 min. The quasispherical morphology products were collected by centrifugation and washed three times with a mixture of deionized (DI) water and ethanol and redispersed in the DI water. The atomic ratio of Au/Cu was controlled by varying the volume of $CuSO_4$ and $HAuCl_4$ solutions (0.1 mL of $CuSO_4$ and 1 mL of $HAuCl_4$ solution for $Au_1Cu_{0.1}$; 0.2 mL of $CuSO_4$ and 1 mL of $HAuCl_4$ solution for $Au_1Cu_{0.2}$; 0.4 mL of $CuSO_4$ and 1 mL of $HAuCl_4$ solution for $Au_1Cu_{0.5}$; 1 mL of $CuSO_4$ and 0.4 mL of $HAuCl_4$ solution for Au_1Cu_1; 1.5 mL of $CuSO_4$ and 1 mL of $HAuCl_4$ solution for Au_1Cu_2).

3.4. Colorimetric Detection of H_2O_2 Using Au–Cu Alloy Nanoparticles as Peroxidase Mimetics

The colorimetric detection process was performed as follows. A total of 30 μL of an aqueous dispersion containing Au–Cu alloy nanoparticles (0.4 mg/mL), 200 μL of TMB solution (2.5 mM), and 200 μL of different concentrations of H_2O_2 were mixed with 1.5 mL of acetate buffer (20 mM, pH 4.0), and the mixture was incubated at room temperature for 120 min. After the reaction, the solution was subjected to UV-VIS absorption spectroscopy analysis.

3.5. Selectivity of H_2O_2 Detection Using Au–Cu Alloy Nanoparticles as Peroxidase Mimetics

An analysis of the selectivity of the H_2O_2 detection by the Au–Cu alloy nanoparticles was performed through the following process. A total of 30 μL of an aqueous dispersion containing Au–Cu alloy nanoparticles (0.4 mg/mL), 200 μL of TMB solution (2.5 mM), and 200 μL of H_2O_2 (10 mM) was added into 1.5 mL of acetate buffer (20 mM, pH 4.0). The resulting solution was then incubated at room temperature for 120 min. For the control experiments under the same conditions, the same number of common ions (Na^+, K^+, Ca^{2+}, Mg^{2+}, PO_4^{3-}, Cl^-) or substances (AA, glucose, urea) as that of H_2O_2 was added to the reaction system.

3.6. Colorimetric Detection and Selectivity Analysis of Glucose Using Au–Cu Nanoparticles as Peroxidase Mimetics

Glucose detection was performed as follows. First, 100 μL of glucose oxidase (GOx) (0.0032 g/mL) and 100 μL of the glucose solution (various concentrations) prepared in the HEPES buffer solution (pH 6.5) were incubated at 37 °C for 30 min. Subsequently, 1.5 mL of the NaOAc buffer solution (pH 4), 100 μL of Au–Cu alloy nanoparticles (0.0004 g/mL), and 200 μL of the TMB (1 mM) solution were added to the above solution. The mixture was incubated at room temperature for 120 min and was further used for performing the absorption spectroscopy measurement. As for the selectivity analysis, the glucose homologues (sucrose, lactose, maltose, and mannitol) were used in control experiments.

4. Conclusions

In this paper, we synthesized five types of Au–Cu alloy nanoparticles with different Au/Cu ratios by a facile coreduction method. The synthesized Au–Cu alloy nanoparticles were able to act as peroxidase mimetics for H_2O_2 and glucose colorimetric detection with a LOD of 0.141 μM and 0.26 μM. Furthermore, it was demonstrated that both the catalytic activity and selectivity of Au-based nanocatalysts were enhanced by mixing Au and Cu into alloy catalysts with specific properties. We expect that the developed method can be extended to prepare other noble-metal-based alloy nanocatalysts.

Supplementary Materials: The following are available online at https://www.mdpi.com/2073-4344/11/3/343/s1, Figure S1. Size distribution of (a) $Au_1Cu_{0.1}$, (b) $Au_1Cu_{0.2}$, (c) $Au_1Cu_{0.5}$, (d) Au_1Cu_1, and (e) Au_1Cu_2 alloy nanoparticles; Figure S2. Energy-dispersive X-ray spectrometry mapping of (a) $Au_1Cu_{0.1}$, (b)$Au_1Cu_{0.2}$, (c) $Au_1Cu_{0.5}$, (d) Au_1Cu_1, and (e) Au_1Cu_2 alloy nanoparticles; Figure S3. Ultraviolet-visible absorption spectra of (a) Au–Cu alloy nanoparticles, (b) Au nanoparticles, and (c) Cu nanoparticles. Figure S4. Ultraviolet-visible absorption spectra of 3,3′,5,5′-tetramethylbenzidine (TMB) solutions in the presence of different concentrations of H_2O_2 using (a) $Au_1Cu_{0.1}$, (b) $Au_1Cu_{0.2}$, (c) $Au_1Cu_{0.5}$, (d) Au_1Cu_1, and (e) Au_1Cu_2 alloy nanoparticles as the peroxi-

dase mimetics; Figure S5. Transmission electron microscopy images of (a) Au nanoparticles and (b) Cu nanoparticles; Figure S6. Ultraviolet-visible absorption spectra of 3,3′,5,5′-tetramethylbenzidine (TMB) solutions in the presence of different concentrations of H_2O_2 using (a) Au nanoparticles and (b) Cu nanoparticles as the peroxidase mimetics; Figure S7. Ultraviolet-visible absorption spectra of 3,3′,5,5′-tetramethylbenzidine (TMB) solutions in the presence of different concentration of glucose using (a) $Au_1Cu_{0.1}$, (b) $Au_1Cu_{0.2}$, (c) $Au_1Cu_{0.5}$, (d) Au_1Cu_1, and (e) Au_1Cu_2 alloy nanoparticles as the peroxidase mimetics. Table S1. Inductively coupled plasma results of Au_xCu_y alloy nanoparticles.

Author Contributions: Conceptualization, synthesis, characterization, catalytic activity assay, and writing—original draft preparation, C.L.; supervision, methodology, further data analysis, and writing—review and editing, S.H.I. and T.Y. All authors have read and agreed to the published version of the manuscript.

Funding: This work was supported by the NRF grant funded by the Korean government (MSIP) (NRF-2014R1A5A1009799, NRF-2020R1A2C1003885, NRF-2019R1A6C1010052, and NRF-2020M3A7B 4002030).

Conflicts of Interest: The authors declare no conflict of interest.

References

1. Jiang, X.Y.; Wang, H.J.; Yuan, R.; Chai, Y.Q. Functional Three-Dimensional Porous Conductive Polymer Hydrogels for Sensitive Electrochemiluminescence in Situ Detection of H_2O_2 Released from Live Cells. *Anal. Chem.* **2018**, *90*, 8462–8469. [CrossRef]
2. Shi, Q.R.; Song, Y.; Zhu, C.Z.; Yang, H.P.; Du, D.; Lin, Y.H. Mesoporous Pt Nanotubes as a Novel Sensing Platform for Sensitive Detection of Intracellular Hydrogen Peroxide. *ACS Appl. Mater. Interfaces* **2015**, *7*, 24288–24295. [CrossRef]
3. Shen, R.; Liu, P.P.; Zhang, Y.Q.; Yu, Z.; Chen, X.Y.; Zhou, L.; Nie, B.Q.; Zaczek, A.; Chen, J.; Liu, J. Sensitive Detection of Single-Cell Secreted H_2O_2 by Integrating a. Microfluidic Droplet Sensor and Au Nanoclusters. *Anal. Chem.* **2018**, *90*, 4478–4484. [CrossRef] [PubMed]
4. Hage, R.; Lienke, A. Applications of transition-metal catalysts to textile and wood-pulp bleaching. *Angew. Chem. Int. Ed.* **2006**, *45*, 206–222. [CrossRef] [PubMed]
5. Ciriminna, R.; Albanese, L.; Meneguzzo, F.; Pagliaro, M. Hydrogen Peroxide: A Key Chemical for Today's Sustainable Development. *Chemsuschem* **2016**, *9*, 3374–3381. [CrossRef]
6. Sun, J.H.; Li, C.Y.; Qi, Y.F.; Guo, S.L.; Liang, X. Optimizing Colorimetric Assay Based on V_2O_5 Nanozymes for Sensitive Detection of H_2O_2 and Glucose. *Sensors* **2016**, *16*, 584. [CrossRef]
7. Baghayeri, M.; Zare, E.N.; Lakouraj, M.M. A simple hydrogen peroxide biosensor based on a novel electro-magnetic poly(p-phenylenediamine) @ Fe_3O_4 nanocomposite. *Biosens. Bioelectron.* **2014**, *55*, 259–265. [CrossRef]
8. Suarez, G.; Santschi, C.; Martin, O.J.F.; Slaveykova, V.I. Biosensor based on chemically designed anchorable cytochrome c for the detection of H_2O_2 released by aquatic cells. *Biosens. Bioelectron.* **2013**, *42*, 385–390. [CrossRef]
9. Lou, Z.R.; Li, P.; Sun, X.F.; Yang, S.Q.; Wang, B.S.; Han, K.L. A fluorescent probe for rapid detection of thiols and imaging of thiols reducing repair and H_2O_2 oxidative stress cycles in living cells. *Chem. Commun.* **2013**, *49*, 391–393. [CrossRef]
10. Liu, G.D.; Lin, Y.H. Amperometric glucose biosensor based on self-assembling glucose oxidase on carbon nanotubes. *Electrochem. Commun.* **2006**, *8*, 251–256. [CrossRef]
11. Gong, T.T.; Liu, J.F.; Wu, Y.W.; Xiao, Y.; Wang, X.H.; Yuan, S.Q. Fluorescence enhancement of CdTe quantum dots by HBcAb-HRP for sensitive detection of H_2O_2 in human serum. *Biosens. Bioelectron.* **2017**, *92*, 16–20. [CrossRef]
12. Dickinson, B.C.; Chang, C.J. A targetable fluorescent probe for imaging hydrogen peroxide in the mitochondria of living cells. *J. Am. Chem. Soc.* **2008**, *130*, 9638–9639. [CrossRef]
13. Nasir, M.; Nawaz, M.H.; Latif, U.; Yaqub, M.; Hayat, A.; Rahim, A. An overview on enzyme-mimicking nanomaterials for use in electrochemical and optical assays. *Microchim. Acta* **2017**, *184*, 323–342. [CrossRef]
14. Lin, T.R.; Zhong, L.S.; Song, Z.P.; Guo, L.Q.; Wu, H.Y.; Guo, Q.Q.; Chen, Y.; Fu, F.F.; Chen, G.N. Visual detection of blood glucose based on peroxidase-like activity of WS2 nanosheets. *Biosens. Bioelectron.* **2014**, *62*, 302–307. [CrossRef] [PubMed]
15. Vazquez-Gonzalez, M.; Liao, W.C.; Gazelles, R.; Wang, S.; Yu, X.; Gutkin, V.; Willner, I. Mimicking Horseradish Peroxidase Functions Using Cu^{2+}-Modified Carbon Nitride Nanoparticles or Cu^{2+}-Modified Carbon Dots as Heterogeneous Catalysts. *ACS Nano* **2017**, *11*, 3247–3253. [CrossRef] [PubMed]
16. Liu, Q.Y.; Yang, Y.T.; Lv, X.T.; Ding, Y.A.; Zhang, Y.Z.; Jing, J.J.; Xu, C.X. One-step synthesis of uniform nanoparticles of porphyrin functionalized ceria with promising peroxidase mimetics for H_2O_2 and glucose colorimetric detection. *Sens. Actuators B Chem.* **2017**, *240*, 726–734. [CrossRef]
17. Yang, H.K.; Xiao, J.Y.; Su, L.; Feng, T.; Lv, Q.Y.; Zhang, X.J. Oxidase-mimicking activity of the nitrogen-doped Fe_3C@C composites. *Chem. Commun.* **2017**, *53*, 3882–3885. [CrossRef]
18. Wulff, G. Enzyme-like catalysis by molecularly imprinted polymers. *Chem. Rev.* **2002**, *102*, 1–27. [CrossRef] [PubMed]

19. He, W.W.; Liu, Y.; Yuan, J.S.; Yin, J.J.; Wu, X.C.; Hu, X.N.; Zhang, K.; Liu, J.B.; Chen, C.Y.; Ji, Y.L.; et al. Au@Pt nanostructures as oxidase and peroxidase mimetics for use in immunoassays. *Biomaterials* **2011**, *32*, 1139–1147. [CrossRef]
20. Singh, S.; Tripathi, P.; Kumar, N.; Nara, S. Colorimetric sensing of malathion using palladium-gold bimetallic nanozyme. *Biosens. Bioelectron.* **2017**, *92*, 280–286. [CrossRef] [PubMed]
21. Jin, L.H.; Meng, Z.; Zhang, Y.Q.; Cai, S.J.; Zhang, Z.J.; Li, C.; Shang, L.; Shen, Y.H. Ultrasmall Pt Nanoclusters as Robust Peroxidase Mimics for Colorimetric Detection of Glucose in Human Serum. *ACS Appl. Mater. Interfaces* **2017**, *9*, 10027–10033. [CrossRef] [PubMed]
22. Liu, J.; Meng, L.J.; Fei, Z.F.; Dyson, P.J.; Jing, X.N.; Liu, X. MnO_2 nanosheets as an artificial enzyme to mimic oxidase for rapid and sensitive detection of glutathione. *Biosens. Bioelectron.* **2017**, *90*, 69–74. [CrossRef] [PubMed]
23. Gao, L.Z.; Zhuang, J.; Nie, L.; Zhang, J.B.; Zhang, Y.; Gu, N.; Wang, T.H.; Feng, J.; Yang, D.L.; Perrett, S.; et al. Intrinsic peroxidase-like activity of ferromagnetic nanoparticles. *Nat. Nanotechnol.* **2007**, *2*, 577–583. [CrossRef]
24. Zhao, H.; Dong, Y.M.; Jiang, P.P.; Wang, G.L.; Zhang, J.J. Highly Dispersed CeO_2 on TiO_2 Nanotube: A Synergistic Nanocomposite with Superior Peroxidase-Like Activity. *ACS Appl. Mater. Interfaces* **2015**, *7*, 6451–6461. [CrossRef]
25. Chen, W.; Chen, J.; Feng, Y.B.; Hong, L.; Chen, Q.Y.; Wu, L.F.; Lin, X.H.; Xia, X.H. Peroxidase-like activity of water-soluble cupric oxide nanoparticles and its analytical application for detection of hydrogen peroxide and glucose. *Analyst* **2012**, *137*, 1706–1712. [CrossRef]
26. Andre, R.; Natalio, F.; Humanes, M.; Leppin, J.; Heinze, K.; Wever, R.; Schroder, H.C.; Muller, W.E.G.; Tremel, W. V_2O_5 Nanowires with an Intrinsic Peroxidase-Like Activity. *Adv. Funct. Mater.* **2011**, *21*, 501–509. [CrossRef]
27. Yan, X.; Song, Y.; Wu, X.L.; Zhu, C.Z.; Su, X.G.; Du, D.; Lin, Y.H. Oxidase-mimicking activity of ultrathin MnO_2 nanosheets in colorimetric assay of acetylcholinesterase activity. *Nanoscale* **2017**, *9*, 2317–2323. [CrossRef] [PubMed]
28. Zhang, Y.F.; Xu, C.L.; Li, B.X.; Li, Y.B. In situ growth of positively charged gold nanoparticles on single-walled carbon nanotubes as a highly active peroxidase mimetic and its application in biosensing. *Biosens. Bioelectron.* **2013**, *43*, 205–210. [CrossRef]
29. Pogacean, F.; Socaci, C.; Pruneanu, S.; Biris, A.R.; Coros, M.; Magerusan, L.; Katona, G.; Turcu, R.; Borodi, G. Graphene based nanomaterials as chemical sensors for hydrogen peroxide—A comparison study of their intrinsic peroxidase catalytic behavior. *Sens. Actuators B Chem.* **2015**, *213*, 474–483. [CrossRef]
30. Han, L.; Li, C.C.; Zhang, T.; Lang, Q.L.; Liu, A.H. Au@Ag Heterogeneous Nanorods as Nanozyme Interfaces with Peroxidase-Like Activity and Their Application for One-Pot Analysis of Glucose at Nearly Neutral pH. *ACS Appl. Mater. Interfaces* **2015**, *7*, 14463–14470. [CrossRef] [PubMed]
31. Chen, X.M.; Tian, X.T.; Su, B.Y.; Huang, Z.Y.; Chen, X.; Oyama, M. Au nanoparticles on citrate-functionalized graphene nanosheets with a high peroxidase-like performance. *Dalton Trans.* **2014**, *43*, 7449–7454. [CrossRef] [PubMed]
32. Li, J.N.; Liu, W.Q.; Wu, X.C.; Gao, X.F. Mechanism of pH-switchable peroxidase and catalase-like activities of gold, silver, platinum and palladium. *Biomaterials* **2015**, *48*, 37–44. [CrossRef]
33. Niu, X.H.; Chen, C.; Zhao, H.L.; Chai, Y.; Lan, M.B. Novel snowflake-like Pt-Pd bimetallic clusters on screen-printed gold nanofilm electrode for H_2O_2 and glucose sensing. *Biosens. Bioelectron.* **2012**, *36*, 262–266. [CrossRef] [PubMed]
34. Lin, Y.H.; Ren, J.S.; Qu, X.G. Nano-Gold as Artificial Enzymes: Hidden Talents. *Adv. Mater. Technol.* **2014**, *26*, 4200–4217. [CrossRef] [PubMed]
35. Wang, S.; Chen, W.; Liu, A.L.; Hong, L.; Deng, H.H.; Lin, X.H. Comparison of the Peroxidase-Like Activity of Unmodified, Amino-Modified, and Citrate-Capped Gold Nanoparticles. *ChemPhysChem* **2012**, *13*, 1199–1204. [CrossRef] [PubMed]
36. Zhang, H.J.; Watanabe, T.; Okumura, M.; Haruta, M.; Toshima, N. Catalytically highly active top gold atom on palladium nanocluster. *Nat. Mater.* **2012**, *11*, 49–52. [CrossRef] [PubMed]
37. Zhang, L.F.; Zhong, S.L.; Xu, A.W. Highly Branched Concave Au/Pd Bimetallic Nanocrystals with Superior Electrocatalytic Activity and Highly Efficient SERS Enhancement. *Angew. Chem. Int. Ed.* **2013**, *52*, 645–649. [CrossRef] [PubMed]
38. Zhang, Q.; Cobley, C.M.; Zeng, J.; Wen, L.P.; Chen, J.Y.; Xia, Y.N. Dissolving Ag from Au-Ag Alloy Nanoboxes with H_2O_2: A Method for Both Tailoring the Optical Properties and Measuring the H_2O_2 Concentration. *J. Phys. Chem. C* **2010**, *114*, 6396–6400. [CrossRef] [PubMed]
39. Li, X.Y.; Du, X.Z. Molybdenum disulfide nanosheets supported Au-Pd bimetallic nanoparticles for non-enzymatic electrochemical sensing of hydrogen peroxide and glucose. *Sens. Actuators B Chem.* **2017**, *239*, 536–543. [CrossRef]
40. Sui, N.; Liu, F.Y.; Wang, K.; Xie, F.X.; Wang, L.N.; Tang, J.J.; Liu, M.H.; Yu, W.W. Nano Au-Hg amalgam for Hg^{2+} and H_2O_2 detection. *Sens. Actuators B Chem.* **2017**, *252*, 1010–1015. [CrossRef]
41. Tang, Z.; Shahzad, A.; Kim, W.S.; Yu, T. Cost-effective aqueous-phase synthesis of long copper nanowires. *RSC Adv.* **2015**, *5*, 83880–83884. [CrossRef]
42. Tang, Z.; Kwon, H.; Yi, M.; Kim, K.; Han, J.W.; Kim, W.S.; Yu, T. Role of halide ions for controlling morphology of copper nanocrystals in aqueous solution. *ChemistrySelect* **2017**, *2*, 4655–4661. [CrossRef]
43. Denton, A.R.; Ashcroft, N.W. Vegard's law. *Phys. Rev. A* **1991**, *43*, 3161. [CrossRef] [PubMed]
44. Liu, Y.; Purich, D.L.; Wu, C.; Wu, Y.; Chen, T.; Cui, C.; Zhang, L.; Cansiz, S.; Hou, W.; Wang, Y.; et al. Ionic Functionalization of Hydrophobic Colloidal Nanoparticles to Form Ionic Nanoparticles with Enzymelike Properties. *J. Am. Chem. Soc.* **2015**, *137*, 14952–14958. [CrossRef]
45. Shrivastava, A.; Gupta, V.B. Methods for the determination of limit of detection and limit of quantitation of the analytical methods. *Chron. Young Sci.* **2011**, *2*, 21. [CrossRef]

46. Sun, Y.; Tian, P.; Ding, D.; Yang, Z.; Wang, W.; Xin, H.; Han, Y.F. Revealing the active species of Cu-based catalysts for heterogeneous Fenton reaction. *Appl. Catal. B* **2019**, *258*, 117985. [CrossRef]
47. Zeng, J.; Zhang, Q.; Chen, J.Y.; Xia, Y.N. A Comparison Study of the Catalytic Properties of Au-Based Nanocages, Nanoboxes, and Nanoparticles. *Nano Lett.* **2010**, *10*, 30–35. [CrossRef] [PubMed]
48. Liu, H.; Ding, Y.N.; Yang, B.C.; Liu, Z.X.; Liu, Q.Y.; Zhang, X. Colorimetric and ultrasensitive detection of H_2O_2 based on Au/Co_3O_4-CeO_x nanocomposites with enhanced peroxidase-like performance. *Sens. Actuators B Chem.* **2018**, *271*, 336–345. [CrossRef]
49. Ding, Y.N.; Yang, B.C.; Liu, H.; Liu, Z.X.; Zhang, X.; Zheng, X.W.; Liu, Q.Y. FePt-Au ternary metallic nanoparticles with the enhanced peroxidase-like activity for ultrafast colorimetric detection of H_2O_2. *Sens. Actuators B Chem.* **2018**, *259*, 775–783. [CrossRef]
50. Chen, J.X.; Wu, W.W.; Huang, L.; Ma, Q.; Dong, S.J. Self-Indicative Gold Nanozyme for H_2O_2 and Glucose Sensing. *Chem. Eur. J.* **2019**, *25*, 11940–11944. [CrossRef]
51. Song, C.; Ding, W.; Zhao, W.W.; Liu, H.B.; Wang, J.; Yao, Y.W.; Yao, C. High peroxidase-like activity realized by facile synthesis of FeS_2 nanoparticles for sensitive colorimetric detection of H_2O_2 and glutathione. *Biosens. Bioelectron.* **2020**, *151*, 111983. [CrossRef] [PubMed]
52. Cao, X.; Wang, N.; Jia, S.; Shao, Y.H. Detection of Glucose Based on Bimetallic PtCu Nanochains Modified Electrodes. *Anal. Chem.* **2013**, *85*, 5040–5046. [CrossRef] [PubMed]
53. Lu, J.; Zhang, H.; Li, S.; Guo, S.; Shen, L.; Zhou, T.; Zhang, Y. Oxygen-vacancy-enhanced peroxidase-like activity of reduced Co_3O_4 nanocomposites for the colorimetric detection of H_2O_2 and glucose. *Inorg. Chem.* **2020**, *59*, 3152–3159. [CrossRef] [PubMed]
54. Yang, H.; Wang, Z.; Li, C.; Xu, C. Nanoporous PdCu alloy as an excellent electrochemical sensor for H_2O_2 and glucose detection. *J. Colloid Interface Sci.* **2017**, *491*, 321–328. [CrossRef] [PubMed]
55. Zhao, D.; Xu, C. A nanoporous palladium-nickel alloy with high sensing performance towards hydrogen peroxide and glucose. *J. Colloid Interface Sci.* **2015**, *447*, 50–57. [CrossRef]
56. Ngamaroonchote, A.; Sanguansap, Y.; Wutikhun, T.; Karn-Orachai, K. Highly branched gold-copper nanostructures for non-enzymatic specific detection of glucose and hydrogen peroxide. *Microchim. Acta* **2020**, *187*, 1–12. [CrossRef]
57. Lee, W.C.; Kim, K.B.; Gurudatt, N.G.; Hussain, K.K.; Choi, C.S.; Park, D.S.; Shim, Y.B. Comparison of enzymatic and non-enzymatic glucose sensors based on hierarchical Au-Ni alloy with conductive polymer. *Biosens. Bioelectron.* **2019**, *130*, 48–54. [CrossRef]
58. Lin, L.; Weng, S.; Zheng, Y.; Liu, X.; Ying, S.; Chen, F.; You, D. Bimetallic PtAu alloy nanomaterials for nonenzymatic selective glucose sensing at low potential. *J. Electroanal. Chem.* **2020**, *865*, 114147. [CrossRef]